

Supplementary Information

Flame made nanoparticles permit processing of dense, flexible, Li⁺ conducting ceramic electrolyte thin films of cubic-Li₇La₃Zr₂O₁₂ (c-LLZO)

Eongyu Yi, Weimin Wang, John Kieffer, and Richard M. Laine*

Energy and/or equipment intensive sintering process of c-LLZO

Table S1. Reported sintering conditions and properties of c-LLZO $\{(Li_{7-2x-y}A_xLa_3Zr_{2-y}B_yO_{12}, (A^{3+}, B^{5+}))\}$.

	Dopant(s)	Sintering condition	% density	RT ionic conductivity (mS cm ⁻¹)	Remark	Ref.
Solid state reaction	n/a	1230 °C / 36 h / air	92	0.24	Likely Al ³⁺ contamination from crucible. Covered in mother powder.	1
	Al ³⁺	1230 °C / 36 h / air	n/a	0.18	Covered in mother powder.	2
	Nb ⁵⁺	1200 °C / 36 h / air	92	0.8	n/a	3
	Ta ⁵⁺	1140 °C / 16 h / air	94	1.02	Covered in mother powder.	4
	Al ³⁺ /Ta ⁵⁺	1140 °C / 9 h / O ₂	96	0.74		5
		Al ³⁺	1100 °C / 12 h / air	92	0.25	Attrition milled (~1µm powder). Covered in mother powder.
Spray pyrolysis	Al ³⁺	1000 °C / 1 h / air	51	0.0044	Fully decomposed starting powder. Covered in mother powder.	7
Sol-gel	Al ³⁺	900 °C / (n/a) / air	n/a	0.0024	Sol-gel dip coating. Li ₂ CO ₃ placed near to retard Li loss.	8
	Al ³⁺	1200 °C / 10 h / air	96	0.61 (33°C)	Li ₄ SiO ₄ sintering additive. Covered in mother powder.	9
Co-precipitation	Nb ⁵⁺	1100 °C / 36 h / air	87	0.52	Covered in mother powder.	10
Pechini method	Al ³⁺	1200 °C / 6 h / air	92	0.2		11
Hot press	Ta ⁵⁺	1050 °C / 1 h / Ar / 62 MPa	98	0.82	Co-precipitation derived powder. No mother powder.	12
	Al ³⁺	1000 °C / 1 h / Ar / 40 MPa	96	0.4	Sol-gel derived powder. No mother powder.	13
	Al ³⁺	1000 °C / 1 h / Ar / 40 MPa	98	0.4	Solid state reaction derived powder. No mother powder.	14
Flame Spray Pyrolysis	Al ³⁺	1090 °C / 1 h / N ₂	94	0.2	Fully decomposed starting powder. No mother powder.	This work

Conventional sintering of c-LLZO requires 10-40 h of dwell at temperatures above 1100 °C where Li easily volatilizes. Furthermore, repeated calcination and ball-milling to obtain powders for pellet compaction are also time and energy intensive. Pellets are covered in mother powder during sintering to reduce Li loss. In contrast, hot-pressing shortens the sintering time to 1 h at lower temperatures of 1000-1050 °C to result in near full densities with the aid of pressure. Note the powders used for hot-pressing are also ball-milled and calcined.

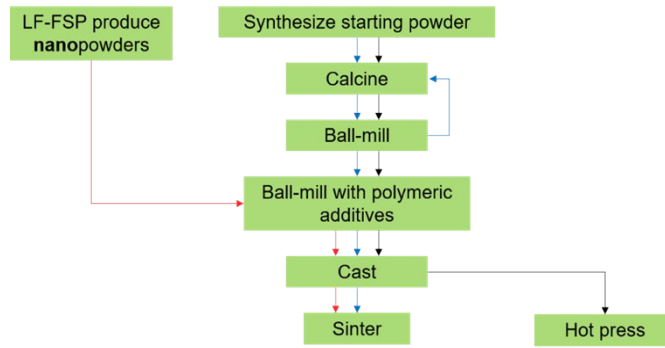


Fig. S1. Comparison of potential processing routes. While there are no reports of successful thin film formulation based on reported approaches so far, paths that would be taken if one were to translate reported methods to sintering films are shown. Direct processing of LF-FSP made nanopowder provides a processing short-cut while significantly reducing required external energy to reach high densities at the same time.

New constraints surface on transferring known approaches to forming thin films. First, mother powder cannot be used, since they will sinter to the films which will be difficult to remove without fracturing the film. For hot-press, the film may crack during sintering due to uneven pressure. Also, even if it is possible to sinter thin films in certain condition there are other limits; scalability, utility in shaping, cost.

From Table S1, it is noted that pentavalent cation doping results in higher conductivities. Please note that the objective of the work reported here is not to obtain highest ionic conductivity but to demonstrate a novel, efficient route to c-LLZO, and also forming thin films by carefully controlling processing variables; starting powder, wet processing, sintering condition.

Morphology and particle size uniformity of LF-FSP made nanopowders

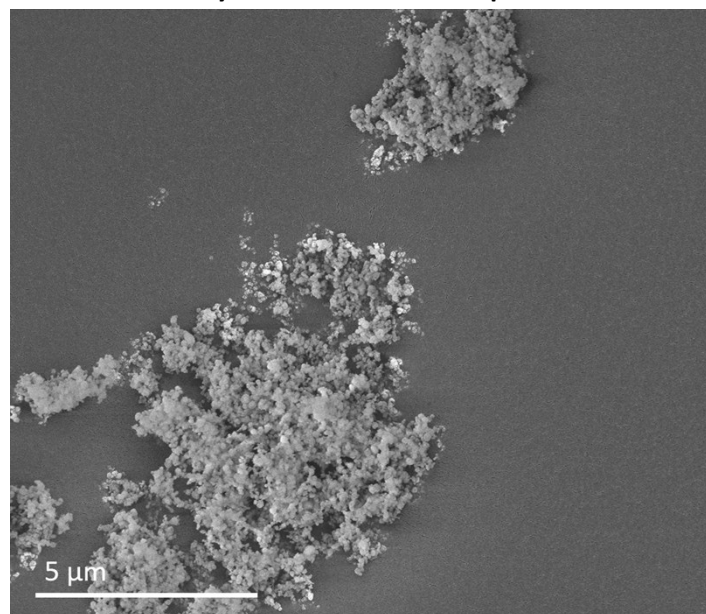


Fig. S2. Low magnification SEM image of as-produced nanopowders. This figure demonstrates that LF-FSP made powders are spherical nanopowders with narrow size distributions. Particles are agglomerated (physically bonded), but not aggregated (chemically bonded).

Determination of the off-stoichiometric $\text{La}_2\text{Zr}_2\text{O}_7$

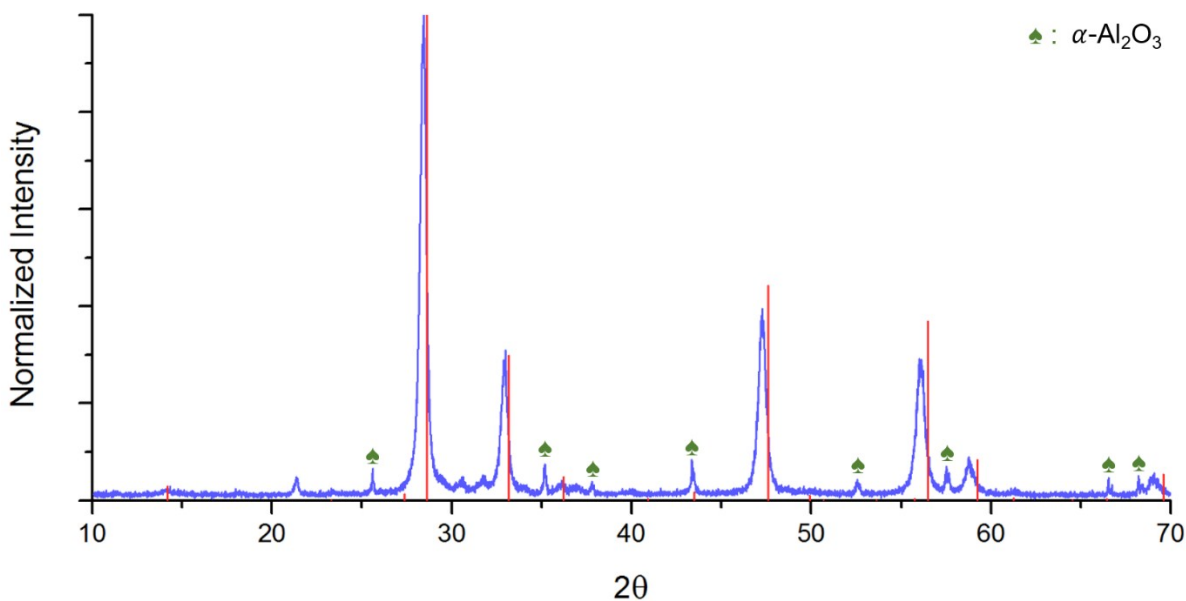


Fig. S3. XRD scan of as-produced LLZO with $\alpha\text{-Al}_2\text{O}_3$ internal standard. An internal standard, $\alpha\text{-Al}_2\text{O}_3$, was mixed with as-produced LLZO using a mortar and pestle. Commonly used internal standard Si metal could not be used as it overlaps with $\text{La}_2\text{Zr}_2\text{O}_7$ peaks. Peak shifts are noted. Observed off-stoichiometric $\text{La}_2\text{Zr}_2\text{O}_7$ peaks are shifted left with respect to stoichiometric $\text{La}_2\text{Zr}_2\text{O}_7$ (red drop lines), indicating larger lattice constants. New lattice constant of 10.87882 \AA was refined using the whole pattern fitting of Jade software. This is larger than the stoichiometric lattice constant, 10.7997 \AA . Hence, the off-stoichiometric composition is $0.43\text{La}_2\text{O}_3\text{-}0.57\text{ZrO}_2$ ($\text{La}_3\text{Zr}_2\text{O}_{8.5}$) which is stable at temperatures of $>1550 \text{ }^\circ\text{C}$ based on the $\text{ZrO}_2\text{-La}_2\text{O}_3$ binary phase diagram.¹⁵ Rapid quenching of LF-FSP gives access to high temperature phases.

Starting materials for suspension formulation

Table S2. Starting materials and composition for suspension formulation.

	Role	Wt.%
LLZO with 2 wt.% polyacrylic acid	Powder/dispersant	37
Benzyl butyl phthalate	Plasticizer	3
Polyvinyl butyral	Binder	3
Ethanol	Solvent	29
Acetone	Solvent	29

Polymeric additives are selected as commonly used binder and plasticizer. Solvent system was selected empirically. All starting materials were added into a 20 ml vial and ball-milled for 12-24 h. ZrO_2 milling media was used to avoid contamination. Sum of wt. % is not 100 due to rounding off.

Thermogravimetric analysis of green films

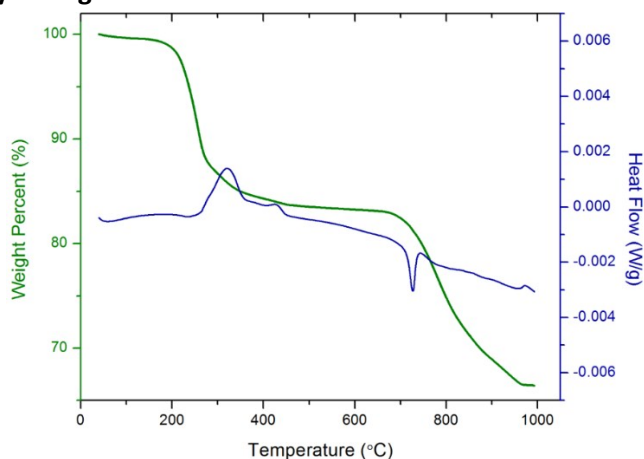


Fig. S4. TGA-DSC of LLZO green film. Initial 2 wt. % mass loss at < 200 °C is ascribed to removal of residual solvent and/or physi-/chemi-sorbed water. Following mass losses with exotherms are due to oxidative decomposition of polymeric additives; dispersant, binder, and plasticizer. Most polymeric additives are oxidatively removed at ~450 °C and the mass remains stable to ~680 °C. An endotherm attributed to melting of Li_2CO_3 is observed near 720 °C accompanied by mass loss as CO_2 evolves, in accordance with the TGA-DSC of the as-produced powder (Fig. 1d). Final ceramic yield is ~66 wt. %, in good agreement with theoretically expected based on Table S2. Note the ceramic yield of LLZO with 2 wt. % PAA dispersant itself is ~77 wt.%.

Tetragonal to cubic phase transition with lithium loss with increasing heating temperatures

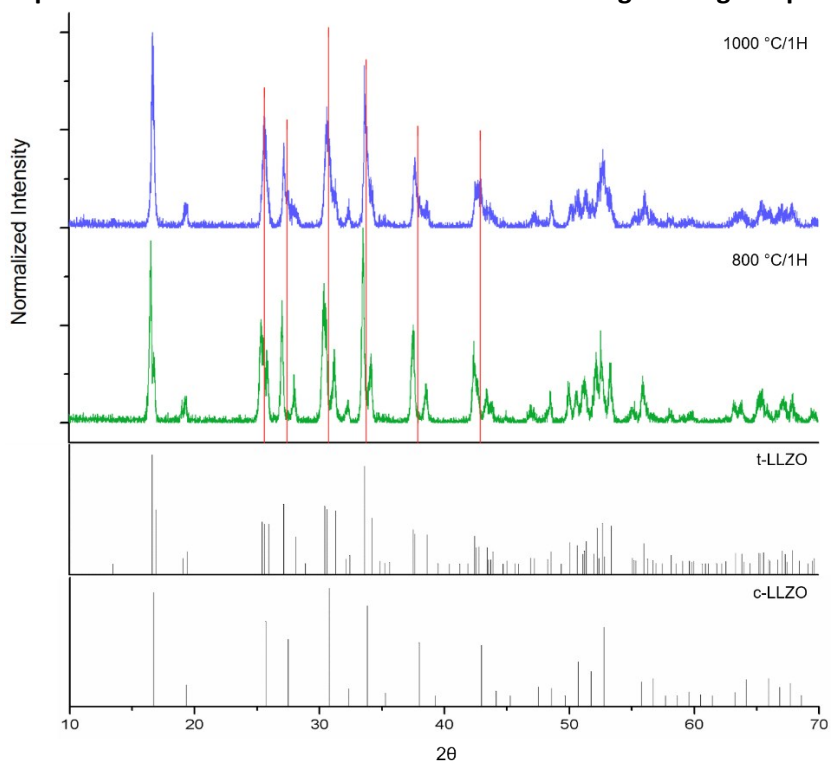


Fig. S5. XRD scans of LLZO films heated to 800 and 1000 °C for 1 h. Film heated to 800 °C/1 h shows mostly t-LLZO whereas on heating to 1000 °C/1 h a mixture of c-LLZO and t-LLZO forms, indicating Li_2O is volatilized at or near 1000 °C. Selected major c-LLZO peaks are marked as red drop lines to mark the difference.

Closer look at c-LLZO films sintered at 1100 °C / 1 h

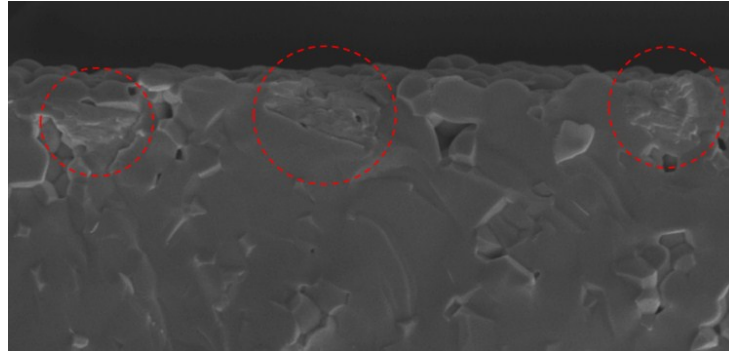


Fig. S6. SEM fracture surface image of c-LLZO film sintered at 1100 °C for 1 h. Circled area show distinctly different microstructural features. It is likely these are the initiation point of secondary phases $\text{La}_2\text{Zr}_2\text{O}_7$ and La_2O_3 as Li_2O is lost at the surface on over-exposure of heat.

Effect of green film thicknesses (Li loss rate) on the microstructure and phase composition

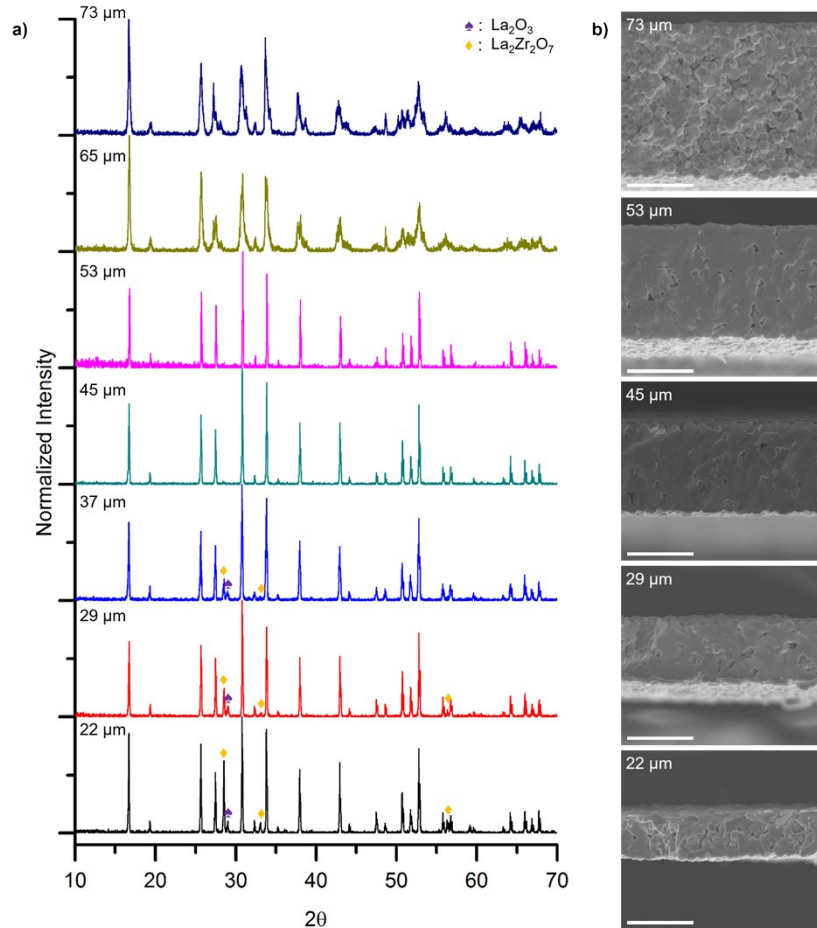


Fig. S7. (a) XRD scans and (b) SEM micrographs of LLZO films with different green film thicknesses heated to 1090 °C for 1 h. Note the thicknesses labelled are green film thicknesses, not sintered film thicknesses. La_2O_3 and $\text{La}_2\text{Zr}_2\text{O}_7$ peak intensities rise with decreasing thickness. Films too thick result in t-LLZO as observed by peak splitting for 65 and 73 μm thick film. Microstructures of sintered films are affected by lithium content as secondary phases, including t-LLZO, have different sintering temperatures compared to c-LLZO. Scale bar, 20 μm for (b).

Ionic conductivities of low relative density c-LLZO thin films

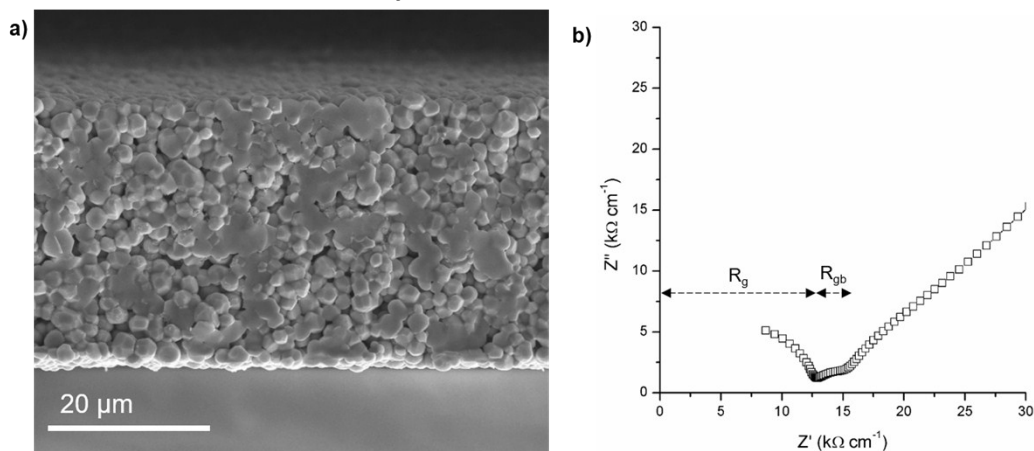


Fig. S8. (a) SEM fracture surface image and (b) Nyquist plot of c-LLZO films heated to below sintering temperature. Films sintered at 1070 °C for 2 h did not fully densify, showing porosity. Mixed inter- and trans-granular fracture modes are observed. XRD confirmed single phase c-LLZO. Nyquist plot shows both grain and grain boundary resistance component. Total ionic conductivity is calculated as $0.07 \pm 0.01 \text{ mS cm}^{-1}$.

References

- 1 R. Murugan, V. Thangadurai, W. Weppner, *Angew. Chem. Int. Ed.* 2007, **46**, 7778-7781.
- 2 M. Kotobuki, H. Munakata, K. Kanamura, Y. Sato, T. Yoshida, *J. Electrochem. Soc.* 2010, **157**, A1076-A1079.
- 3 S. Ohta, T. Kobayashi, T. Asaoka, *J. Power Sources* 2011, **196**, 3342-3345.
- 4 K. Liu, C.-A. Wang, *Electrochem. Commun.* 2014, **48**, 147-150.
- 5 Y. Li, Z. Wang, C. Li, Y. Cao, X. Guo, *J. Power Sources* 2014, **248**, 642-646.
- 6 L. Cheng, W. Chen, M. Kunz, K. Persson, N. Tamura, G. Chen, M. Doeff, *ACS Appl. Mater. Interfaces* 2015, **7**, 2073-2081.
- 7 R. Djenadic, M. Botros, C. Benel, O. Clemens, S. Indris, A. Choudhary, T. Bergfeldt, H. Hahn, *Solid State Ionics* 2014, **263**, 49-56.
- 8 K. Tadanaga, H. Egawa, A. Hayashi, M. Tatsumisago, J. Mosa, M. Aparicio, A. Duran, *J. Power Sources* 2015, **273**, 844-847.
- 9 N. Janani, C. Deviannapoorani, L. Dhivya, R. Murugan, *RSC Adv.* 2014, **4**, 51228-51238.
- 10 H. Imagawa, S. Ohta, Y. Kihira, T. Asaoka, *Solid State Ionics* 2014, **262**, 609-612.
- 11 Y. Jin, P.J. McGinn, *J. Power Sources* 2011, **196**, 8683-8687.
- 12 T. Thompson, A. Sharafi, M.D. Johannes, A. Huq, J.L. Allen, J. Wolfenstine, J. Sakamoto, *Adv. Energy Mater.* 2015, **5**, 1500096.
- 13 J. Sakamoto, E. Rangasamy, H. Kim, Y. Kim, J. Wolfenstine, *Nanotechnology* 2013, **24**, 424005.
- 14 E. Rangasamy, J. Wolfenstine, J. Sakamoto, *Solid State Ionics* 2012, **206**, 28-32.
- 15 R.S. Roth, *J. Res. Natl. Bur. Stand.* 1956, **56**, 17-25.